

Critical Phase Dualities in 1D Exactly Solvable Quasiperiodic Models


Miguel Gonçalves^{1,2}, Bruno Amorim³, Eduardo V. Castro^{2,4} and Pedro Ribeiro^{1,4}

¹*CeFEMA-LaPMET, Departamento de Física, Instituto Superior Técnico, Universidade de Lisboa, Avenida Rovisco Pais, 1049-001 Lisboa, Portugal*

²*Centro de Física das Universidades do Minho e Porto, LaPMET, Departamento de Física e Astronomia, Faculdade de Ciências, Universidade do Porto, 4169-007 Porto, Portugal*

³*Centro de Física das Universidades do Minho e Porto, LaPMET, University of Minho, Campus of Gualtar, 4710-057 Braga, Portugal*

⁴*Beijing Computational Science Research Center, Beijing 100193, China*

 (Received 13 September 2022; accepted 25 September 2023; published 3 November 2023)

We propose a solvable class of 1D quasiperiodic tight-binding models encompassing extended, localized, and critical phases, separated by nontrivial mobility edges. Limiting cases include the Aubry-André model and the models of Sriram Ganeshan, J. H. Pixley, and S. Das Sarma [*Phys. Rev. Lett.* **114**, 146601 (2015)] and J. Biddle and S. Das Sarma [*Phys. Rev. Lett.* **104**, 070601 (2010)]. The analytical treatment follows from recognizing these models as a novel type of fixed points of the renormalization group procedure recently proposed in *Phys. Rev. B* **108**, L100201 (2023) for characterizing phases of quasiperiodic structures. Beyond known limits, the proposed class of models extends previously encountered localized-delocalized duality transformations to points within multifractal critical phases. Besides an experimental confirmation of multifractal duality, realizing the proposed class of models in optical lattices allows stabilizing multifractal critical phases and nontrivial mobility edges in an undriven system without the need for the unbounded potentials required by previous proposals.

DOI: [10.1103/PhysRevLett.131.186303](https://doi.org/10.1103/PhysRevLett.131.186303)

Quasiperiodic systems (QPSs) offer a rich playground of interesting physics ranging from exotic localization properties in one [1–6] or higher [7–14] dimensions, to intriguing topological properties [15–19]. Quasiperiodicity has been studied in widely different platforms, including optical [2,4,5,20–26] and photonic lattices [3,12,15,17,27–29], cavity-polariton devices [30], phononic media [31–36], moiré materials [37], periodically and quasiperiodically driven systems [38–44], and non-Hermitian quasicrystals [45–51]. The ubiquity of QPSs and their relevance to several interdisciplinary topical issues rendered these systems a hot topic of research.

QPSs host phases with fully localized and extended wave functions. Interestingly, quasiperiodicity can also stabilize critical multifractal states, first encountered at the localization-delocalization transition lines, and later found to persist over extended regions [40,52–58].

QPSs present substantial challenges for theoretical methods, and an analytical treatment of the localization phase diagrams remains restricted to a few fine-tuned models [1,53,59–63], and even a smaller subset hosts critical phases [53,57], that have been a subject of very recent experimental interest [64]. In particular, Ref. [53] found critical phases with energy-independent transitions to localized and delocalized phases, i.e., without mobility edges. These were shown to be robust to interactions, giving rise to many-body critical regimes [65] and have been simulated using ultracold

atoms [66]. In Ref. [57] mobility edges were reported, however, requiring unbounded potentials. Examples of coexistence of extended, critical, and localized regimes, separated by mobility edges, were reported in Ref. [67], but only numerically. As the existence of energy-dependent critical-to-extended or critical-to-localized transitions has not been experimentally reported so far, more models with such physics, no need for diverging potentials, and with analytically exact phase diagrams, are of topical and practical interest for experimental implementations.

Here, we propose a class of 1D quasiperiodic tight-binding models that includes extended, localized, and critical phases and determine its phase diagram analytically in the thermodynamic limit. Physically motivated by previous experimental realizations in optical lattices, our models contain exponentially decaying hoppings and quasiperiodic harmonics, with a tunable decay length. As limiting cases, this class contains the Aubry-André model and the model in Ref. [63], that were already experimentally realized [2,25], and the model in Ref. [60]. Away from these limits, our class of models contains novel features, not found in any of the limiting cases: critical phases that extend over a considerable region of parameters and energy-dependent transitions between critical and extended or localized phases.

The main results are shown in Fig. 1. In Fig. 1(a), we show numerical and analytical results for the phase diagram, for a fixed set of parameters, where a critical phase exists over a

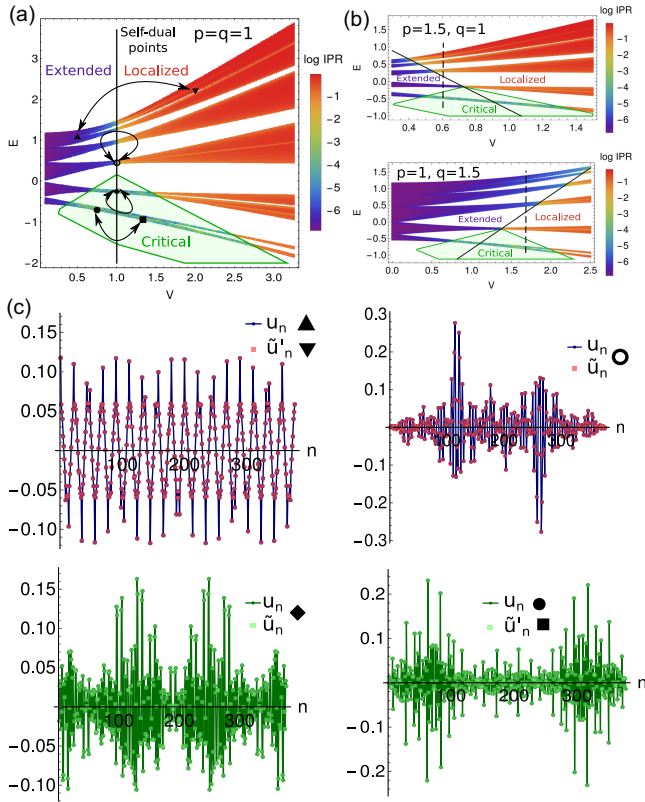


FIG. 1. (a) IPR [see below Eq. (2) for definition] results obtained numerically for $L = F_{16} = 987$, $p = q = 1$ and as a function of the strength of the quasiperiodic potential V [see Eq. (1)]. Superimposed are the analytical extended-localized phase boundaries (SD points) and the critical phase (bounded by green lines). (b) Phase diagrams obtained for $p = 1.5$, $q = 1$ (up) and $p = 1$, $q = 1.5$ (down). The dashed lines indicate values of V for which all the phases can be reached at different energies. (c) Examples of eigenstates u_n and dual eigenstates \tilde{u}_n defined in Eq. (4) at dual points in the phase diagram indicated in (a), for $L = F_{14} = 377$. Since $p = q$, $W(x) = 1$ and \tilde{u}'_n and u_n are simply related by the Aubry-André duality.

wide range of the quasiperiodic potential strength V [see Eq. (1)]. The phase diagram hosts exact dualities that are more general than the ones previously found for the limiting models in Refs. [60,63]. They exist not only between the extended and localized phase and at the self-dual (SD) transition points, but also within the critical phase. Examples are shown in Fig. 1(c), where the real-space wave function amplitude u_n at site n , is exactly equal to its dual \tilde{u}_n [see Eq. (4) for definition], at dual points in the phase diagram marked in Fig. 1(a). In Fig. 1(b), we also show that highly tunable mobility edges between extended and localized phases can be introduced by choosing different decay lengths for the hoppings and quasiperiodic harmonics. Interestingly, we can have all the phases, including the critical phase, arising at different energies for a fixed set of parameters, as also shown in Fig. 1(b).

Model and methods.—We consider a family of models parameterized by the Hamiltonian

$$H = t \sum_{n \neq n'} e^{i\alpha(n-n')} e^{-p|n-n'|} c_n^\dagger c_{n'} + 2V \sum_n \sum_{l=1}^{+\infty} e^{-ql} \cos[l(2\pi\tau n + \phi)] c_n^\dagger c_n \quad (1)$$

where c_n^\dagger creates a particle at site n . The first term describes hoppings modulated by a magnetic flux α with an exponential decay determined by p . The second term represents a quasiperiodic potential, incommensurate with the lattice for $\tau \neq \mathbb{Q}$, obtained by summing harmonics of the incommensurate wave number $2\pi\tau$ with exponentially decaying amplitudes controlled by the parameter q . In the following we set $t = 1$ unless otherwise stated. The model in Eq. (1) reduces to that in [60] in the $q \rightarrow \infty$ limit and $\alpha = 0$ after replacing $t \rightarrow te^p$ and $V \rightarrow Ve^q$. Similarly, it reduces to the model in [63] for large p , and to the Aubry-André model when both p and q are large.

We consider finite systems with L sites. In order to avoid boundary defects, we consider rational approximants of the irrational parameter τ . We chose $1/\tau$ as the golden ratio in the numerical calculations, but our analytical results for the phase diagram are independent of τ . The rational approximants are written as $\tau_c^{(n)} = F_{n-1}/F_n$, where F_n is a Fibonacci number defining the number of sites L in the unit cell, with $L = F_n$ [68,69]. We impose twisted boundary conditions, with phase twists k which is the same as working in a fixed momentum sector of the Hamiltonian in the Bloch basis defined as $c_n \rightarrow c_{m,r} = N^{-1/2} \sum_k e^{ik(m+rL)} \tilde{c}_{m,k}$, where $m = 0, \dots, L-1$ runs over the L sites of the unit cell, and $r = 0, \dots, N$ is the unit cell index, with $N \rightarrow \infty$ the total number of unit cells. The Hamiltonian for a fixed k sector becomes

$$H(k) = t \sum_{r=-\infty}^{\infty} \sum_{m,m'=0}^{L-1} e^{-p|rL+m-m'|} e^{i(\alpha-k)(m+rL-m')} \tilde{c}_{m,k}^\dagger \tilde{c}_{m',k} + 2V \sum_{m=0}^{L-1} \sum_{l=1}^{+\infty} e^{-ql} \cos[l(2\pi\tau_c m + \phi)] \tilde{c}_{m,k}^\dagger \tilde{c}_{m,k}. \quad (2)$$

which is just the Hamiltonian of a system with L sites and a phase twist k . For the analytical calculations, we study commensurate approximants (CAs) defined by $\tau_c = L'/L$, where L' and L are coprime integers, in the $L \rightarrow \infty$ limit (infinite unit cell size or quasiperiodic limit). In particular, we use the methods introduced in Ref. [70] and an exact generalized duality that we prove below.

Our analytical results are confirmed numerically through the real-space and momentum-space inverse participation ratios, respectively, IPR and IPR_k . For an eigenstate $|\psi(E)\rangle = \sum_n \psi_n(E) |n\rangle$, where $\{|n\rangle\}$ is a basis localized at each site, these quantities are defined as $\text{IPR}_{(k)}(E) = (\sum_n |\psi_n^{(k)}(E)|^2)^{-2} \sum_n |\psi_n^{(k)}(E)|^4$ [71], where $\psi_n^{(k)}(E)$ are the amplitudes of the discrete Fourier transform of the set

$\{\psi_n(E)\}$. In the extended phase, the IPR scales as L^{-1} and IPR_k is L independent, while in the localized phase, the IPR scales as L^{-1} while the IPR is L independent (for large enough L). At a critical point or critical phase, the wave function is multifractal: it is delocalized in real and momentum space and both the IPR and IPR_k scale down with L [71].

Exact duality.—The Schrödinger equation for the model in Eq. (2) with phase twists k can be written as

$$h_n u_n - \sum_{m=-\infty}^{\infty} e^{i(\alpha-k)(n-m)} e^{-p|n-m|} u_m = 0, \quad (3)$$

where $h_n = \eta - V\chi(q, 2\pi\tau n + \phi)$, $\eta = E + t + V$ and $\chi(\lambda, x) = \sum_l e^{-\lambda|l|} e^{ilx} = \sinh(\lambda) [\cosh(\lambda) - \cos(x)]^{-1}$. At dual points $P(t, V, p, q, \alpha, E; \phi, k)$ and $P'(t', V', p', q', \alpha', E'; \phi', k')$, this equation can be mapped into a dual equation under the duality transformation (see Ref. [72] for proof):

$$\tilde{u}_n = \sum_m e^{i2\pi\tau nm} W(2\pi\tau m) u_m, \quad (4)$$

where $W(x) = \chi(q', x + \phi') \chi^{-1}(p, x + k - \alpha)$. The dual points P and P' satisfy

$$\begin{aligned} \phi' &= k - \alpha + \pi \frac{(s-1)}{2}, \\ -k' + \alpha' &= \phi + \pi \frac{(s-1)}{2} \\ \frac{D(V', \eta', p', q')}{B(V', \eta', p')} &= s \frac{D(V, \eta, p, q)}{A(V, \eta, q)}; \\ \frac{A(V', \eta', q')}{B(V', \eta', p')} &= \frac{B(V, \eta, p)}{A(V, \eta, q)} \\ \frac{\eta'}{B(V', \eta', p')} &= s \frac{\eta}{A(V, \eta, q)} \end{aligned} \quad (5)$$

where $s = \pm 1$ and

$$\begin{aligned} A(V, \eta, q) &= -\eta \cosh q + V \sinh q \\ B(V, \eta, p) &= -\eta \cosh p + t \sinh p \\ D(V, \eta, p, q) &= \eta \cosh p \cosh q - t \cosh q \sinh p \\ &\quad - V \cosh p \sinh q. \end{aligned} \quad (6)$$

For fixed $p = q$, Eq. (4) defines the usual Aubry-André duality. The self-duality condition is imposed by choosing $P = P'$. In this case, Eq. (5) is solved simply through the condition $A(V, \eta, q) = \pm B(V, \eta, p)$, that yields the following equation for the SD points:

$$E = \frac{V \sinh q \mp t \sinh p}{\cosh q \mp \cosh p} - t - V. \quad (7)$$

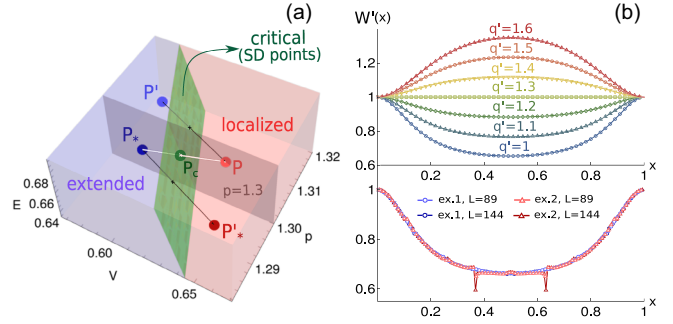


FIG. 2. (a) Example of globally dual points obeying the global duality in Eq. (4) (sets of points $P \leftrightarrow P'$ and $P_* \leftrightarrow P'_*$ connected by black lines), locally dual points obeying local hidden dualities ($P \leftrightarrow P_*$ connected by white line, belonging to plane $p = 1.3$), and a SD critical point P_c . For this figure, we have set $q = q' = 1$. (b) Top: duality function $W'(x) \propto W(2\pi x)$ for a point P defined by $p = 1.3$, $q = 1$, $V \approx 0.73$, $E \approx 0.34$, and different dual points parameterized by different values of q' (the remaining dual parameters, V' , p' and E' were obtained by solving Eq. (5) for the different choices of q'). The data points correspond to the $L = 55$ samples of the duality function $W'(x)$ obtained for a CA with $\tau_c = 34/55$ (see Ref. [72] for details). The full lines are plots of the exact analytical duality function in Eq. (4). The latter was normalized so that $W(0) = W'(0)$. Bottom: examples of samples of $W'(x)$ for different locally dual points within the plane $p = 1.3$, for $\tau_c = 55/89$ and $\tau_c = 89/144$ (the energies for the different CAs were chosen to be the closest possible to each other).

Examples of dual points are shown in Fig. 2(a). Points P and P' are globally dual, being described by the duality transformation in Eq. (4), as well as points P_* and P'_* . However, local dualities can also arise close to the SD points even along directions in the parameter space where the global duality breaks down [73]. Examples are the points P_* and P in Fig. 2(a). These locally dual points are defined by invariant local energy dispersions under the interchange $k \leftrightarrow \phi$, but only for large enough L [73].

The global duality transformation defined in Eq. (4) was confirmed to match the definition given in Ref. [73] in terms of CAs. Given dual points in the phase diagram, the definition introduced in Ref. [73] allows, for a given CA, to calculate L samples of the associated duality function $W'(x) \propto W(2\pi x)$ at points $x_n = \text{mod}(\tau_c n / L, 1)$, $n = 0, \dots, L-1$ (see Ref. [72], Sec. S2 for details). Figure 2(b) (top) shows perfect agreement between the exact global duality function $W(x)$ in Eq. (4) and the samples of duality function $W'(x)$ computed through a CA with $L = 55$ sites. The results were obtained by choosing a fixed point P and different dual points P' defined by varying q' . This illustrates that even though P is fixed, the duality transformation depends on its dual point P' (in particular on q'), in accordance with the definition in Eq. (4), a feature that is absent in previously found exact duality transformations [60,63]. Finally, Fig. 2(b) (bottom) shows examples of duality functions $W'(x)$ obtained at

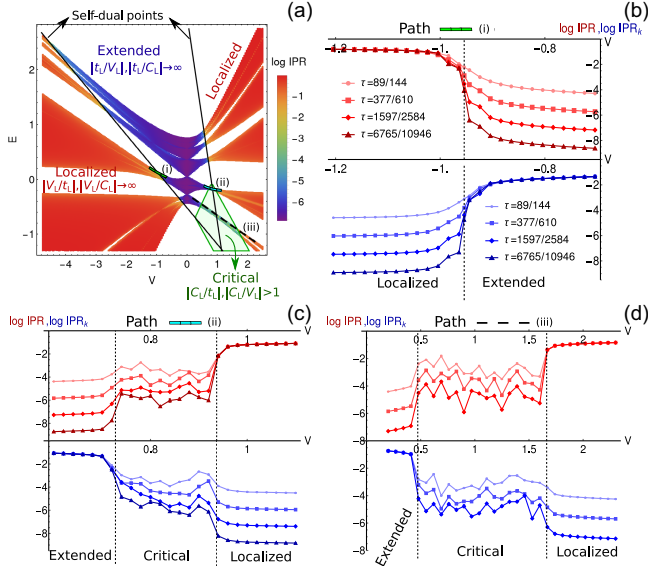


FIG. 3. (a) IPR results obtained for $p = 1.3$, $q = 1$, and $L = F_{16} = 987$, superimposed with the analytical curves for SD points (black) and phase boundaries of the critical phase (green). In each phase, we also show the asymptotic results of the renormalized couplings as $L \rightarrow \infty$. (b)–(d) Finite-size scalings of the IPR (red) and IPR_k (blue) for points (V, E) across the paths shown in the dashed curves in (a). The results were averaged over 70, 25, 16, and 6 random shifts ϕ and twists k , respectively, for increasing $L \in [144, 10946]$. The dashed vertical lines correspond to the analytical results for the phase boundaries.

locally dual points, being nonsmooth for specific values of x , as previously found for other models [73,74].

Phase diagram.—We now analytically obtain the complete phase diagram. The transitions between extended and localized phases obtained through the IPR/ IPR_k calculations perfectly match the SD points described by Eq. (7). Examples are shown in Fig. 1(a) for $p = q$, when Eq. (7) reduces to the Aubry-André energy independent SD line $V = t$, and Figs. 3(a) and 3(b) for $p \neq q$. However, the SD points can also occur within the critical phase, in which case they are not associated with any transition. This implies that the phase boundaries of the critical phase are not described by SD points.

To obtain the full phase diagram analytically we make use of the renormalization-group approach developed in Ref. [70]. In fact, the model studied here is a fixed-point model according to the classification in [70]. Its characteristic polynomial $\mathcal{P}_L(\varphi, \kappa) \equiv \det[H_L(\varphi, \kappa) - E]$, with $H_L(\varphi, \kappa)$ the Hamiltonian for a CA with L sites, is (see Ref. [72])

$$\mathcal{P}_L(\varphi, \kappa) = V_L \cos(\varphi) + t_L \cos(\kappa) + C_L \cos(\varphi) \cos(\kappa) + D_L, \quad (8)$$

where $\varphi = L\phi$, $\kappa = Lk$, and V_L , t_L , C_L and D_L are renormalized couplings. For the simplest CA (one site

per unit cell), we have, using the definitions in Eq. (6), that $t_1 = A(V, \eta, q)$, $V_1 = B(V, \eta, p)$, $C_1 = \eta$, and $D_1 = D(V, \eta, p, q)$. The ratios between the renormalized couplings V_L , t_L , and C_L can be computed exactly. If $|t_1/C_1| > 1$ or $|V_1/C_1| > 1$, we have, respectively,

$$\left| \frac{t_L}{C_L} \right| = \frac{|g_L^+(\frac{t_1}{C_1}) + g_L^-(\frac{t_1}{C_1})|}{2}, \quad \left| \frac{V_L}{C_L} \right| = \frac{|g_L^+(\frac{V_1}{C_1}) + g_L^-(\frac{V_1}{C_1})|}{2}, \quad (9)$$

where $g_L^\pm(x) = (x \pm \sqrt{x^2 - 1})^L$. On the other hand, if $|C_1/t_1| > 1$ or $|C_1/V_1| > 1$ we have, respectively,

$$|t_L/C_L| = |T_L(t_1/C_1)|; \quad |V_L/C_L| = |T_L(V_1/C_1)|, \quad (10)$$

where $T_L(x)$ is the L th order Chebyshev polynomial. It is easy to see that if $|t_1/V_1|, |t_1/C_1| > 1$ we have that $|t_L/V_L|, |t_L/C_L| \rightarrow \infty$ exponentially in L as $L \rightarrow \infty$, i.e., we are in the extended phase. For $|V_1/t_1|, |V_1/C_1| > 1$, we have $|V_L/t_L|, |V_L/C_L| \rightarrow \infty$ and the phase is localized. Finally, $|C_1/t_1|, |C_1/V_1| > 1$ ensures that $|C_L/t_L|, |C_L/V_L| > 1$ for any L (a property of Chebyshev polynomials), and the system is in a critical phase. Therefore, the phases and phase boundaries are fully determined through the previous conditions by knowing the functions in Eq. (6). Summarizing, phases and phase boundaries are analytically given by

$$\begin{aligned} |A/B|, |A/\eta| > 1, & \quad \text{ext} \\ |B/A|, |B/\eta| > 1, & \quad \text{loc} \\ |\eta/A|, |\eta/B| > 1, & \quad \text{crit} \end{aligned} \quad (11)$$

$$\begin{aligned} |A| = |B|, |A|, |B| > |\eta|, & \quad \text{ext to loc} \\ |A| = |\eta|, |A|, |\eta| > |B|, & \quad \text{crit to ext} \\ |B| = |\eta|, |B|, |\eta| > |A|, & \quad \text{crit to loc}, \end{aligned} \quad (12)$$

where we omitted the parameter dependence for clarity. From the ratios of renormalized couplings we are also able to calculate the correlation lengths in the extended and localized phases in terms of A , B , and η (see Ref. [72]). Note that the $L \rightarrow \infty$ limit defines the phase diagram for any τ because the renormalized couplings only depend on L .

To confirm our analytical results, we show in Figs. 3(b)–3(d) some examples of finite-size scaling results that agree with the analytical phase boundaries here unveiled. Note that while in the extended-to-localized transitions both the IPR and IPR_k scale down only at the critical point [Fig. 3(b)], such scaling is observed for the entire range of the critical phase when the latter exists [Figs. 3(c) and 3(d)]. In [72] we also carried out a multifractal

analysis at some points in the critical phase to show the nonlinear behavior of the fractal dimension that characterizes multifractal phases [75].

Discussion.—We analytically obtained the phase diagram of the richest family of 1D quasiperiodic solvable models, to our knowledge, hosting (i) critical multifractal phases in addition to localized and extended ones, and energy-dependent transitions between all these phases; and (ii) a rich generalized duality symmetry that includes dualities inside the critical phase.

From a practical perspective, the family of models we propose can be experimentally realized with currently available techniques. The model in [63] has exactly the quasiperiodic potential considered here and was already experimentally realized using a synthetic lattice of laser-coupled momentum modes [25]. Our model simply requires additional longer-range hoppings (but still exponentially decaying), a possibility put forward in [76]. It can also be simulated in conventional optical lattices, where the exponential hopping decay rate can be directly estimated [60]. A single incommensurate potential (our large q limit) was already realized in optical lattices by applying a second laser beam with a wave vector τ that is incommensurate with that of the primary lattice. Additional quasiperiodic harmonics can be introduced by adding new laser beams with wave vectors that are multiples of τ , as proposed in [63]. The engineering of optical lattices with kicked kinetic energy or quasiperiodic potential is also a possible way to implement our model, as proposed in [57]. An advantage of our model is that the critical multifractal phase can be realized without the need of unbounded potentials. We also note that the existence of exact dualities has direct experimental relevance: critical-extended transitions are dual of critical-localized transitions, implying that the detailed experimental characterization of one transition can give us information on both. The impact of interactions on the phase diagram of this model is an interesting question for future research.

The authors M. G. and P. R. acknowledge partial support from Fundação para a Ciência e Tecnologia (FCT-Portugal) through Grant No. UID/CTM/04540/2019. B. A., E. V. C., and M. G. acknowledge partial support from FCT-Portugal through Grant No. UIDB/04650/2020. M. G. acknowledges further support from FCT-Portugal through the Grant No. SFRH/BD/145152/2019. B. A. acknowledges further support from FCT-Portugal through Grant No. CEECIND/02936/2017. We finally acknowledge the Tianhe-2JK cluster at the Beijing Computational Science Research Center (CSRC) and the OBLIVION supercomputer through Projects No. 2022.15834.CPCA.A1 and No. 2022.15910.CPCA.A1 (based at the High Performance Computing Center—University of Évora) funded by the ENGAGE SKA Research Infrastructure (Reference No. POCI-01-0145-FEDER-022217—COMPETE 2020

and the Foundation for Science and Technology, Portugal) and by the BigData@UE project (Reference No. ALT20-03-0246-FEDER-000033—FEDER) and the Alentejo 2020 Regional Operational Program. Computer assistance was provided by CSRC and the OBLIVION support team.

-
- [1] S. Aubry and G. André, *Proceedings of the VIII International Colloquium on Group-Theoretical Methods in Physics*, Annals of the Israel Physical Society (Hilger, Bristol, 1980), Vol. 3.
 - [2] G. Roati, C. D’Errico, L. Fallani, M. Fattori, C. Fort, M. Zaccanti, G. Modugno, M. Modugno, and M. Inguscio, *Nature (London)* **453**, 895 (2008).
 - [3] Y. Lahini, R. Pugatch, F. Pozzi, M. Sorel, R. Morandotti, N. Davidson, and Y. Silberberg, *Phys. Rev. Lett.* **103**, 013901 (2009).
 - [4] M. Schreiber, S. S. Hodgman, P. Bordia, H. P. Lüschen, M. H. Fischer, R. Vosk, E. Altman, U. Schneider, and I. Bloch, *Science* **349**, 842 (2015).
 - [5] H. P. Lüschen, S. Scherg, T. Kohlert, M. Schreiber, P. Bordia, X. Li, S. Das Sarma, and I. Bloch, *Phys. Rev. Lett.* **120**, 160404 (2018).
 - [6] D. S. Borgnia, A. Vishwanath, and R.-J. Slager, *Phys. Rev. B* **106**, 054204 (2022).
 - [7] C. Huang, F. Ye, X. Chen, Y. V. Kartashov, V. V. Konotop, and L. Torner, *Sci. Rep.* **6**, 32546 (2016).
 - [8] J. H. Pixley, J. H. Wilson, D. A. Huse, and S. Gopalakrishnan, *Phys. Rev. Lett.* **120**, 207604 (2018).
 - [9] M. J. Park, H. S. Kim, and S. B. Lee, *Phys. Rev. B* **99**, 245401 (2019).
 - [10] B. Huang and W. V. Liu, *Phys. Rev. B* **100**, 144202 (2019).
 - [11] Y. Fu, E. J. König, J. H. Wilson, Y.-Z. Chou, and J. H. Pixley, *npj Quantum Mater.* **5**, 71 (2020).
 - [12] P. Wang, Y. Zheng, X. Chen, C. Huang, Y. V. Kartashov, L. Torner, V. V. Konotop, and F. Ye, *Nature (London)* **577**, 42 (2020).
 - [13] M. Gonçalves, H. Z. Olyaei, B. Amorim, R. Mondaini, P. Ribeiro, and E. V. Castro, *2D Mater.* **9**, 011001 (2022).
 - [14] P. Bordia, H. Lüschen, S. Scherg, S. Gopalakrishnan, M. Knap, U. Schneider, and I. Bloch, *Phys. Rev. X* **7**, 041047 (2017).
 - [15] Y. E. Kraus, Y. Lahini, Z. Ringel, M. Verbin, and O. Zeitler, *Phys. Rev. Lett.* **109**, 106402 (2012).
 - [16] Y. E. Kraus and O. Zeitler, *Phys. Rev. Lett.* **109**, 116404 (2012).
 - [17] M. Verbin, O. Zeitler, Y. E. Kraus, Y. Lahini, and Y. Silberberg, *Phys. Rev. Lett.* **110**, 076403 (2013).
 - [18] O. Zeitler, *Opt. Mater. Express* **11**, 1143 (2021).
 - [19] D. S. Borgnia and R.-J. Slager, *Phys. Rev. B* **107**, 085111 (2023).
 - [20] D. J. Boers, B. Goedeke, D. Hinrichs, and M. Holthaus, *Phys. Rev. A* **75**, 063404 (2007).
 - [21] M. Modugno, *New J. Phys.* **11**, 033023 (2009).
 - [22] H. Yao, H. Khoudli, L. Bresque, and L. Sanchez-Palencia, *Phys. Rev. Lett.* **123**, 070405 (2019).
 - [23] H. Yao, T. Giamarchi, and L. Sanchez-Palencia, *Phys. Rev. Lett.* **125**, 060401 (2020).

- [24] R. Gautier, H. Yao, and L. Sanchez-Palencia, *Phys. Rev. Lett.* **126**, 110401 (2021).
- [25] F. A. An, K. Padavić, E. J. Meier, S. Hegde, S. Ganeshan, J. H. Pixley, S. Vishveshwara, and B. Gadway, *Phys. Rev. Lett.* **126**, 040603 (2021).
- [26] T. Kohler, S. Scherg, X. Li, H. P. Lüschen, S. Das Sarma, I. Bloch, and M. Aidelsburger, *Phys. Rev. Lett.* **122**, 170403 (2019).
- [27] M. Verbin, O. Zilberberg, Y. Lahini, Y. E. Kraus, and Y. Silberberg, *Phys. Rev. B* **91**, 064201 (2015).
- [28] A. D. Sinelnik, I. I. Shishkin, X. Yu, K. B. Samusev, P. A. Belov, M. F. Limonov, P. Ginzburg, and M. V. Rybin, *Adv. Opt. Mater.* **8**, 2001170 (2020).
- [29] P. Wang, Q. Fu, R. Peng, Y. V. Kartashov, L. Torner, V. V. Konotop, and F. Ye, *Nat. Commun.* **13**, 6738 (2022).
- [30] V. Goblot, A. Štrkalj, N. Pernet, J. L. Lado, C. Dorow, A. Lemaître, L. Le Gratiet, A. Harouri, I. Sagnes, S. Ravets, A. Amo, J. Bloch, and O. Zilberberg, *Nat. Phys.* **16**, 832 (2020).
- [31] D. J. Apigo, W. Cheng, K. F. Dobiszewski, E. Prodan, and C. Prodan, *Phys. Rev. Lett.* **122**, 095501 (2019).
- [32] X. Ni, K. Chen, M. Weiner, D. J. Apigo, C. Prodan, A. Alù, E. Prodan, and A. B. Khanikaev, *Commun. Phys.* **2**, 55 (2019).
- [33] W. Cheng, E. Prodan, and C. Prodan, *Phys. Rev. Lett.* **125**, 224301 (2020).
- [34] Y. Xia, A. Erturk, and M. Ruzzene, *Phys. Rev. Appl.* **13**, 014023 (2020).
- [35] Z.-G. Chen, W. Zhu, Y. Tan, L. Wang, and G. Ma, *Phys. Rev. X* **11**, 011016 (2021).
- [36] M. Gei, Z. Chen, F. Bosi, and L. Morini, *Appl. Phys. Lett.* **116**, 241903 (2020).
- [37] L. Balents, C. R. Dean, D. K. Efetov, and A. F. Young, *Nat. Phys.* **16**, 725 (2020).
- [38] T. Čadež, R. Mondaini, and P. D. Sacramento, *Phys. Rev. B* **96**, 144301 (2017).
- [39] S. Roy, I. M. Khaymovich, A. Das, and R. Moessner, *SciPost Phys.* **4**, 025 (2018).
- [40] T. Čadež, R. Mondaini, and P. D. Sacramento, *Phys. Rev. B* **99**, 014301 (2019).
- [41] P. Bordia, H. Lüschen, U. Schneider, M. Knap, and I. Bloch, *Nat. Phys.* **13**, 460 (2017).
- [42] M. Sarkar, R. Ghosh, A. Sen, and K. Sengupta, *Phys. Rev. B* **103**, 184309 (2021).
- [43] P. T. Dumitrescu, J. G. Bohnet, J. P. Gaebler, A. Hankin, D. Hayes, A. Kumar, B. Neyenhuis, R. Vasseur, and A. C. Potter, *Nature (London)* **607**, 463 (2022).
- [44] T. Shimasaki, M. Prichard, H. E. Kondakci, J. Pagett, Y. Bai, P. Dotti, A. Cao, T.-C. Lu, T. Grover, and D. M. Weld, *arXiv:2203.09442*.
- [45] H. Jiang, L.-J. Lang, C. Yang, S.-L. Zhu, and S. Chen, *Phys. Rev. B* **100**, 054301 (2019).
- [46] S. Longhi, *Phys. Rev. Lett.* **122**, 237601 (2019).
- [47] K. Kawabata, K. Shiozaki, M. Ueda, and M. Sato, *Phys. Rev. X* **9**, 041015 (2019).
- [48] Y. Liu, Y. Wang, X.-J. Liu, Q. Zhou, and S. Chen, *Phys. Rev. B* **103**, 014203 (2021).
- [49] Y. Liu, Q. Zhou, and S. Chen, *Phys. Rev. B* **104**, 024201 (2021).
- [50] Y. Liu, Y. Wang, Z. Zheng, and S. Chen, *Phys. Rev. B* **103**, 134208 (2021).
- [51] Q. Lin, T. Li, L. Xiao, K. Wang, W. Yi, and P. Xue, *Phys. Rev. Lett.* **129**, 113601 (2022).
- [52] W. DeGottardi, D. Sen, and S. Vishveshwara, *Phys. Rev. Lett.* **110**, 146404 (2013).
- [53] F. Liu, S. Ghosh, and Y. D. Chong, *Phys. Rev. B* **91**, 014108 (2015).
- [54] J. Wang, X.-J. Liu, G. Xianlong, and H. Hu, *Phys. Rev. B* **93**, 104504 (2016).
- [55] X. Deng, S. Ray, S. Sinha, G. V. Shlyapnikov, and L. Santos, *Phys. Rev. Lett.* **123**, 025301 (2019).
- [56] Y. Wang, L. Zhang, S. Niu, D. Yu, and X.-J. Liu, *Phys. Rev. Lett.* **125**, 073204 (2020).
- [57] T. Liu, X. Xia, S. Longhi, and L. Sanchez-Palencia, *SciPost Phys.* **12**, 27 (2022).
- [58] J. Fraxanet, U. Bhattacharya, T. Grass, M. Lewenstein, and A. Dauphin, *Phys. Rev. B* **106**, 024204 (2022).
- [59] M. Johansson and R. Riklund, *Phys. Rev. B* **43**, 13468 (1991).
- [60] J. Biddle and S. Das Sarma, *Phys. Rev. Lett.* **104**, 070601 (2010).
- [61] J. D. Bodyfelt, D. Leykam, C. Danieli, X. Yu, and S. Flach, *Phys. Rev. Lett.* **113**, 236403 (2014).
- [62] C. Danieli, J. D. Bodyfelt, and S. Flach, *Phys. Rev. B* **91**, 235134 (2015).
- [63] S. Ganeshan, J. H. Pixley, and S. Das Sarma, *Phys. Rev. Lett.* **114**, 146601 (2015).
- [64] T. Shimasaki, M. Prichard, H. E. Kondakci, J. Pagett, Y. Bai, P. Dotti, A. Cao, T.-C. Lu, T. Grover, and D. M. Weld, *arXiv:2203.09442*.
- [65] Y. Wang, C. Cheng, X.-J. Liu, and D. Yu, *Phys. Rev. Lett.* **126**, 080602 (2021).
- [66] T. Xiao, D. Xie, Z. Dong, T. Chen, W. Yi, and B. Yan, *Science bulletin* **66**, 2175 (2021).
- [67] Y. Wang, L. Zhang, W. Sun, and X.-J. Liu, *Phys. Rev. B* **106**, L140203 (2022).
- [68] M. Y. Azbel, *Phys. Rev. Lett.* **43**, 1954 (1979).
- [69] M. Kohmoto, *Phys. Rev. Lett.* **51**, 1198 (1983).
- [70] M. Gonçalves, B. Amorim, E. V. Castro, and P. Ribeiro, *Phys. Rev. B* **108**, L100201 (2023).
- [71] C. Aulbach, A. Wobst, G.-L. Ingold, P. Hänggi, and I. Varga, *New J. Phys.* **6**, 70 (2004).
- [72] See Supplemental Material at <http://link.aps.org/supplemental/10.1103/PhysRevLett.131.186303> for I. Derivation of the generalized global duality transformation; II. Details on the calculation of local dualities using commensurate approximants; III. Derivation of ratios between renormalized couplings; and IV. Multifractal analysis.
- [73] M. Gonçalves, B. Amorim, E. V. Castro, and P. Ribeiro, *SciPost Phys.* **13**, 046 (2022).
- [74] The local duality function may be very sensitive to the choice of the correct dual points. Since their computation was done numerically, there is an associated error. Therefore we slightly varied the computed dual point and checked that some features may arise only due to a slightly incorrect choice of this point (see Ref. [72]).
- [75] M. Janssen, *Int. J. Mod. Phys. B* **08**, 943 (2004).
- [76] B. Gadway, *Phys. Rev. A* **92**, 043606 (2015).